www.shd.org.rs

Journal of the Serbian Chemical Society

JSCS@tmf.bg.ac.yu • www.shd.org.rs/JSCS

J. Serb. Chem. Soc. *74* (1) 71–84 (2009)
JSCS–3810

UDC 537.622.4.004.12:546.47–31+546.711–31
Original scientific paper

Ferromagnetic behaviour of the Zn–Mn–O system

BRANKA BABIĆ-STOJIĆ*, DUŠAN MILIVOJEVIĆ and JOVAN BLANUŠA

Vinča Institute of Nuclear Sciences, P.O. Box 522, 11001 Belgrade, Serbia

(Received 26 May, revised 16 July 2008)

Abstract: Polycrystalline Zn–Mn–O samples with nominal manganese concentrations x = 0.01, 0.04 and 0.10 were synthesized by a solid state reaction route using $(ZnC_2O_4{\cdot}2H_2O)_{1-x}$ and $(MnC_2O_4{\cdot}2H_2O)_x$. Thermal treatment of the samples was performed in air at temperatures 673, 773, 873, 973 and 1173 K for x = 0.01 and at the temperature 773 K for x = 0.04 and 0.10. The samples were investigated by X-ray diffraction, thermogravimetry, differential thermal analysis, transmission electron microscopy, magnetization measurements and electron paramagnetic resonance. X-Ray diffraction was also performed on MnO_2 thermally treated at temperatures 673, 773, 873, 973, 1073 and 1173 K. Room temperature ferromagnetism was observed in the Zn–Mn–O samples with x = 0.01 thermally treated at low temperatures (673 and 773 K) and in the sample with x = 0.04 thermally treated at 773 K. It seems that the ferromagnetic phase could originate from interactions between Mn^{2+} and acceptor defects incorporated in the ZnO crystal lattice during the thermal treatment of the samples.

Keywords: ZnO; diluted magnetic semiconductors; room temperature ferromagnetism.

INTRODUCTION

Semiconductor materials that exhibit ferromagnetism above room temperature (RT) have attracted considerable interest in the past few years. These materials are essential components for the development of spintronic devices. Dietl *et al.*[1] predicted the existence of ferromagnetism with a Curie temperature, T_C, above RT in *p*-type ZnO and GaN doped with Mn. A ferromagnetic phase in undoped carrier and in *n*-type ZnO substituted with Fe, Co and Ni was also predicted.[2,3] Since then, transition metal doped II–VI and III–V semiconductors have been intensively investigated. Among these materials, Mn-doped ZnO is particularly interesting because of its unusual magnetic properties and disagreement about both the existence and the origin of RT ferromagnetism. The first observation of RT ferromagnetism in low-temperature processed bulk and thin

* Corresponding author. E-mail: babic@vin.bg.ac.yu
doi: 10.2298/JSC0901071B

film samples of Mn-doped ZnO was reported by Sharma *et al*.[4] In this study, the authors found that their results were in agreement with a model of carrier induced ferromagnetic ordering between Mn ions in ZnO. The theoretical prediction that *p*-type defects in Mn-substituted ZnO can produce high T_C ferromagnetism was confirmed experimentally by doping Mn^{2+}:ZnO with nitrogen.[5] It was also shown that *n*-type defects in Mn^{2+}:ZnO introduced by Zn vapour diffusion[5] or by hydrogen annealing[6] did not stabilize long range Mn–Mn ferromagnetic coupling. Contrary to these reports, several authors suggested that the high-temperature ferromagnetism in low-temperature processed Mn–Zn–O samples originated from an oxygen-vacancy-stabilized metastable phase, $Mn_{2-x}Zn_xO_{3-\delta}$.[7,8] In addition, some recent studies showed the absence of ferromagnetic ordering in bulk single phase $Zn_{1-x}Mn_xO$ materials down to 2 K.[9–11] Controversial results have also been obtained for $Zn_{1-x}Mn_xO$ thin film samples, which extend from paramagnetic,[12] to spin-glass behaviour,[13] and to low-temperature ferromagnetism.[14] Various properties obtained for the Zn–Mn–O system by different methods suggest a strong dependence of the magnetic properties of these materials on the synthesis conditions. In the present work, we have studied the structural and magnetic properties of Zn–Mn–O samples prepared by thermal treatment in air at various temperatures were studied in order to obtain a better insight into the processes responsible for the observed high-temperature ferromagnetism in this material.

EXPERIMENTAL

Polycrystalline samples of Zn–Mn–O were prepared by a solid-state reaction method using zinc oxalate dihydrate ($ZnC_2O_4{\cdot}2H_2O$, 99.999 %, Alfa Aesar) and manganese oxalate dihydrate ($MnC_2O_4{\cdot}2H_2O$, 99 %, Alfa Aesar) as starting materials. Appropriate amounts of $(ZnC_2O_4{\cdot}2H_2O)_{1-x}$ and $(MnC_2O_4{\cdot}2H_2O)_x$ were mixed, pressed into pellets and calcined at 673 K for 5 h in air. The calcined samples were reground, pelletized and thermally treated at 673, 773, 873, 973 and 1173 K for 12 h in air to obtain Zn–Mn–O samples with a nominal manganese concentration $x = 0.01$. Thermal treatment of the samples with the nominal manganese concentration $x = 0.04$ and 0.10, was carried out at 773 K. The samples of manganese dioxide (MnO_2, 99.999 %, Sigma Aldrich) were thermally treated at 673, 773, 873, 973, 1073 and 1173 K for 12 h in air.

Powder X-ray diffraction (XRD) patterns were recorded on a Philips PW 1050 diffractometer using CuK_α radiation. The XRD patterns were measured with a step size (2θ) of 0.02° at a slow scan rate of 60 s per step. Thermogravimetry (TG) and differential thermal analysis (DTA) were performed by heating up to 1273 K in a static air atmosphere at a heating rate 10° min^{-1} using a model STA-1000 instrument (Stanton-Redcroft) which enables the simultaneous recording of TG and DTA signals. Transmission electron microscopy (TEM) measurements of Zn–Mn–O samples were performed using a Philips EM 400 instrument with an operating voltage 120 kV. The samples were prepared by placing a drop of an aqueous Zn–Mn–O solution onto a carbon-coated copper grid. After drying, the samples were examined by TEM. The magnetization measurements performed using a SQUID magnetometer (MPMS XL-5, Quantum Design). Electron paramagnetic resonance (EPR) experiments were performed on a Varian E-line spectrometer operating at a nominal frequency of 9.5 GHz.

RESULTS AND DISCUSSION

The XRD patterns of Zn–Mn–O samples with a nominal manganese concentration x = 0.01 thermally treated at 673, 773, 873, 973 and 1173 K in air are presented in Fig. 1. The diffraction lines can be indexed based on a mixture of phases, the major phase ZnO and the minor phases MnO_2, Mn_2O_3, Mn_3O_4 and an impurity phase $Zn_{1-y}Mn_yMn_2O_4$ with tetragonal symmetry (space group $I4_1/amd$). The vertical ticks and indices indicate the peak positions for the wurtzite crystal structure of ZnO (space group $P6_3$ mc). The XRD patterns show the evolution of minority manganese oxides phases with increasing temperature of thermal treatment. The XRD pattern of the sample thermally treated at 673 K shows, in addition to the ZnO phase, the presence of MnO_2 and the onset of the Mn_2O_3 phase in the form of a shoulder on the high-angle side of the ZnO (100) peak. In the x = 0.01 sample sintered at 773 K, the Mn_2O_3 phase progressively develops, existing together with MnO_2. With increasing sintering temperature (973 K), the Mn_2O_3 phase did not exhibit a further increase, whereas the impurity phase $Zn_{1-y}Mn_yMn_2O_4$ continued to grow. For a sintering temperature 1173 K, a peak corresponding to the Mn_3O_4 phase appears.

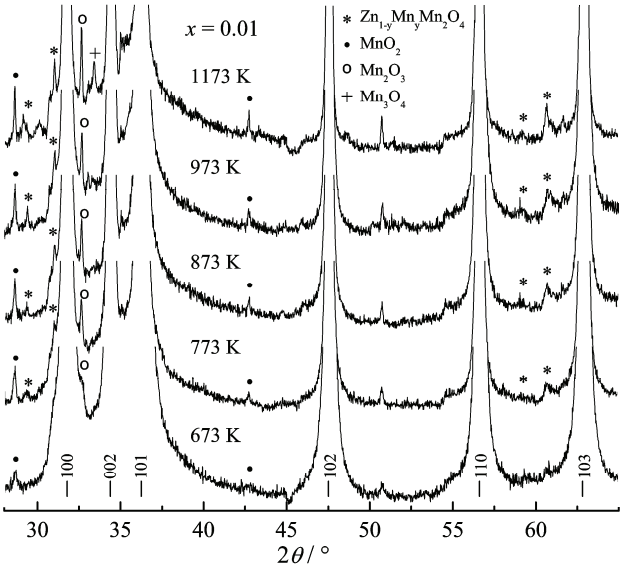

Fig. 1. X-Ray diffraction patterns at 300 K for the Zn–Mn–O samples with x = 0.01, thermally treated at temperatures 673–1173 K recorded at a slow scan rate. The peak positions for the wurtzite ZnO structure are labelled by vertical ticks and indices. Full circles, open circles, "plus" symbol and asterisks in the spectra denote the secondary phases MnO_2, Mn_2O_3,Mn_3O_4 and $Zn_{1-y}Mn_yMn_2O_4$, respectively.

The XRD pattern of the sample with a nominal manganese concentration x = 0.10 thermally treated at 773 K in air is shown in Fig. 2, in which the impurity phase is

clearly observed. All the impurity XRD lines in this spectrum are indexed to $ZnMn_2O_4$, also with tetragonal symmetry (space group $I4_1/amd$). The appearance of an impurity phase with the spinel structure $(Zn_{1-x}Mn(II)_x)[Mn(III)_2]O_4$ having cubic symmetry was detected in Mn-doped ZnO nanoparticles prepared by a co-precipitation method after annealing the 2 and 5 % Mn-doped samples at temperatures $1075 < T < 1275$ K.[15] The tetragonal phase of $ZnMn_2O_4$ was observed in a ZnMnO bulk sample with 1 % Mn sintered in air at 1173 K.[8] The appearance of the $ZnMn_2O_4$ phase in our Zn–Mn–O samples at a temperature of thermal treatment as low as 773 K was probably the result of the fast decomposition of the starting materials used in the synthesis.

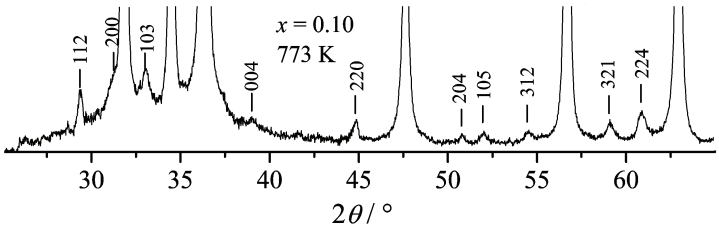

Fig. 2. X-Ray diffraction pattern at 300 K for the Zn–Mn–O sample with $x = 0.10$ thermally treated at 773 K recorded at a slow scan rate. The vertical ticks and indices in the spectrum indicate the peak positions of tetragonal $ZnMn_2O_4$.

The XRD data were subject to Rietveld analysis. The ZnO lattice parameters of the dominant crystal phase in all the samples thermally treated at 773 K were found to be very close to the crystal lattice parameters of ZnO, $a = 3.250$ Å and $c = 5.207$ Å.[16] Changes of the a and c parameters with increasing temperature of thermal treatment from 673 to 1173 K are also not significant. These results are consistent with earlier observations that the solubility of Mn in the ZnO crystal lattice is low.[8,10] The average ZnO crystallite size determined from the width of the X-ray diffraction lines using the Scherrer formula was found to increase with increasing sintering temperature: $d \approx 30$, 50, 70, 70 and 100 nm for the $x = 0.01$ sample thermally treated at 673, 773, 873, 973 and 1173 K, respectively.

The XRD spectra of MnO_2 untreated and thermally treated 12 h in air at 673, 773, 873, 973, 1073 and 1173 K are presented in Fig. 3. Up to 673 K, MnO_2 is stable. At the temperature of 773 K, the Mn_2O_3 phase developed and the sample consisted of equal proportions of MnO_2 and Mn_2O_3 (Fig. 4). At 873 K, the MnO_2 sample was completely transformed into Mn_2O_3 and at 1173 K, the Mn_3O_4 phase appears.

The TG and DTA curves for the oxalate precursors and for a sample of unsintered mixture of $(ZnC_2O_4{\cdot}2H_2O)_{1-x}$ and $(MnC_2O_4{\cdot}2H_2O)_x$ with $x = 0.01$ are presented in Fig. 5. The thermal decomposition of $ZnC_2O_4{\cdot}2H_2O$ occurred in two stages, Fig. 5a. The first stage was dehydration (an endothermic process with $T_{max} = 425$ K). The second stage was the decomposition of anhydrous zinc oxa-

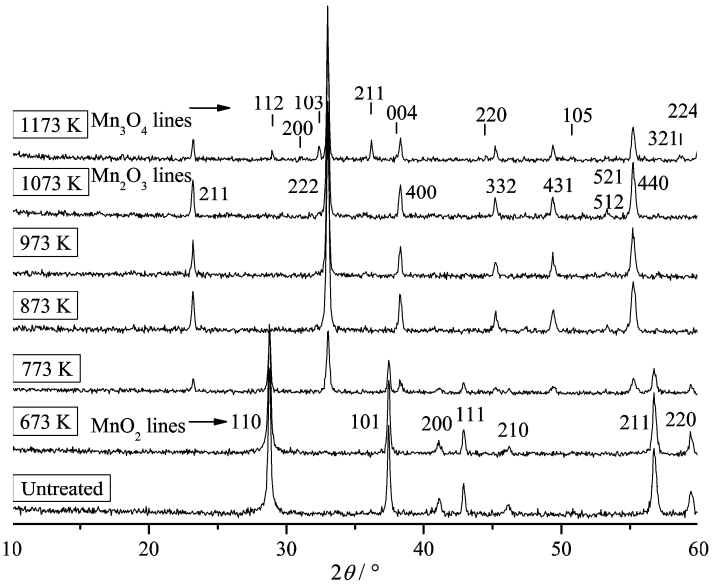

Fig. 3. X-Ray diffraction patterns at 300 K for MnO_2 untreated and thermally treated at temperatures 673–1173 K. The vertical ticks and indices indicate the peak positions of the corresponding manganese oxide noted on the left.

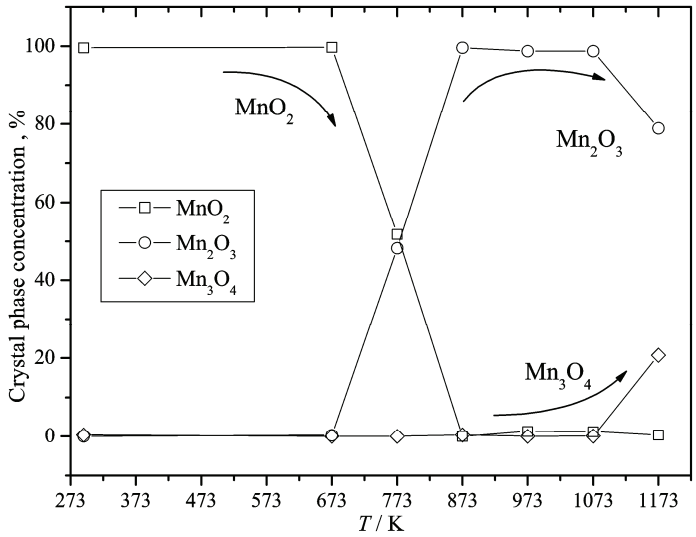

Fig. 4. Relative fraction of various manganese oxides developed after thermal treatment of MnO_2 at temperatures 673–1173 K.

late (an exothermic process with T_{max} = 683 K). The final solid product of this decomposition, found by XRD, was ZnO. The thermal decomposition of the unsintered mixture of two oxalates with x = 0.01 occurred in three stages, Fig. 5b.

The first process was dehydration of the oxalates in the unsintered $x = 0.01$ sample ($T_{max} = 430$ K). The event around $T_{max} = 686$ K involved decomposition of the zinc oxalate phase, and the process around $T_{max} = 598$ K was due to decarbonisation of the manganese oxalate in the sample. The same process of decarbonisation of the manganese oxalate in the starting $MnC_2O_4{\cdot}2H_2O$ material occurred around $T_{max} = 592$ K, as can be seen in Fig. 5c. Taking into consideration the TG/DTA and XRD measurements, it appears that the ZnO phase in the studied Zn–Mn–O samples arose as a product of the decomposition of $ZnC_2O_4{\cdot}2H_2O$, whereas the MnO_2 phase detected in the $x = 0.01$ sample arose as a product of the decomposition of $MnC_2O_4{\cdot}2H_2$ O.

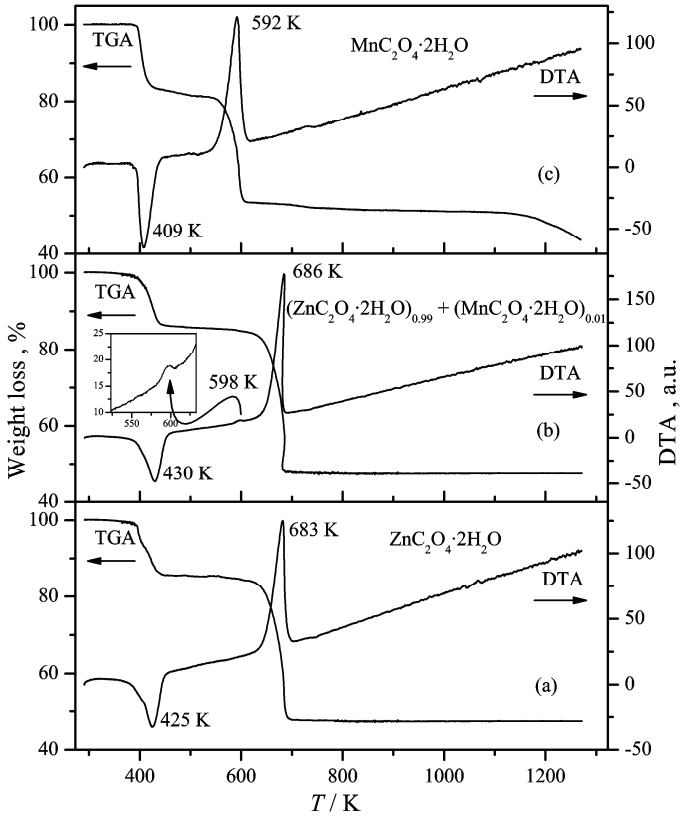

Fig. 5. TG and DTA curves for: $ZnC_2O_4{\cdot}2H_2O$ (a), unsintered mixture of $(ZnC_2O_4{\cdot}2H_2O)_{1-x} + (MnC_2O_4{\cdot}2H_2O)_x$ with $x = 0.01$ (b) and $MnC_2O_4{\cdot}2H_2O$ (c).

The particle size and morphology of one selected sample were characterized by transmission electron microscopy. A typical bright-field TEM image of the Zn–Mn–O sample, with $x = 0.01$, thermally treated at 773 K is shown in Fig. 6. TEM Analysis clearly revealed the presence of two types of particles: one was elongated with a faceted morphology and the other was nearly spherical in shape.

This implies that the two phases can be distinguished. The first is a hexagonal phase corresponding to ZnO recorded by XRD. The size of the ZnO crystallites with faceted morphology seen by TEM lies in the range 50–100 nm, which is consistent with the result obtained from the XRD patterns. The crystallites of the second phase in the TEM image appear in the form of nearly spherical particles. Most of the crystallites of nearly spherical shape have dimensions about 50 nm. These crystallites are attributed to the MnO_2 phase observed in the XRD spectrum of the $x = 0.01$ sample, Fig. 1. A more detailed TEM analysis of the $x = 0.01$ sample thermally treated at 773 K enabled the clarification of the coalescence of some ZnO and MnO_2 crystallites. The observed locations of coalescence of the two phases are denoted by arrows in Fig. 6.

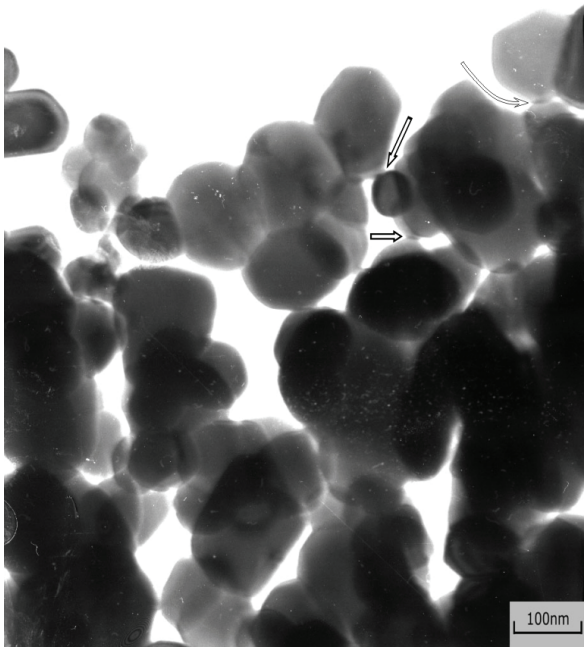

Fig. 6. TEM Microphotograph of the $x = 0.01$ sample thermally treated at 773 K. The arrows in microphotograph denote the locations of coalescence of zinc oxide and manganese oxide crystallites.

The temperature dependence of magnetization under a magnetic field of 500 Oe for the Zn–Mn–O samples with $x = 0.01$, 0.04 and 0.10 thermally treated in air at 773 K for 12 h is presented in Fig. 7. At higher temperatures the magnetization of the $x = 0.01$ sample was larger than that for the $x = 0.04$ and 0.10 samples. The sample with $x = 0.01$ showed a maximum in its $M(T)$ dependence at about 65 K where the $x = 0.04$ and 0.10 samples show a kink.

The magnetic field dependence of magnetization for the $x = 0.01$ sample thermally treated at 673 K was observed at $T = 250$ K (Fig. 8, curve 1) with a coercive field $H_c = 80$ Oe and a remanent magnetization $M_r = 0.0001$ emu/g. The $M(H)$ dependence measured at 300 K for the $x = 0.01$ sample thermally treated at

773 K was characterized by H_c = 800 Oe and M_r = 0.0050 emu/g (Fig. 8, curve 2). Subtracting the paramagnetic component from the total magnetization for the x = 0.01 samples thermally treated at 673 and 773 K, the ferromagnetic component of the magnetization was evaluated with saturation value M_S = 0.0004 emu/g and M_S = 0.0195 emu/g for temperatures 673 and 773 K, respectively (Fig. 8). It can be seen that in the x = 0.01 sample thermally treated at 773 K, the coercive field is ten times larger and saturation magnetization is about fifty times larger than the corresponding values for the sample thermally treated at 673 K.

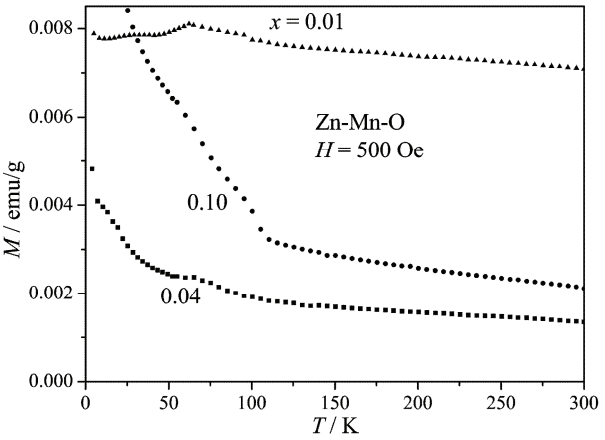

Fig. 7. Temperature dependence of the magnetization in the ZFC state at 500 Oe for Zn–Mn–O samples thermally treated at 773 K, with x = 0.01, 0.04 and 0.10.

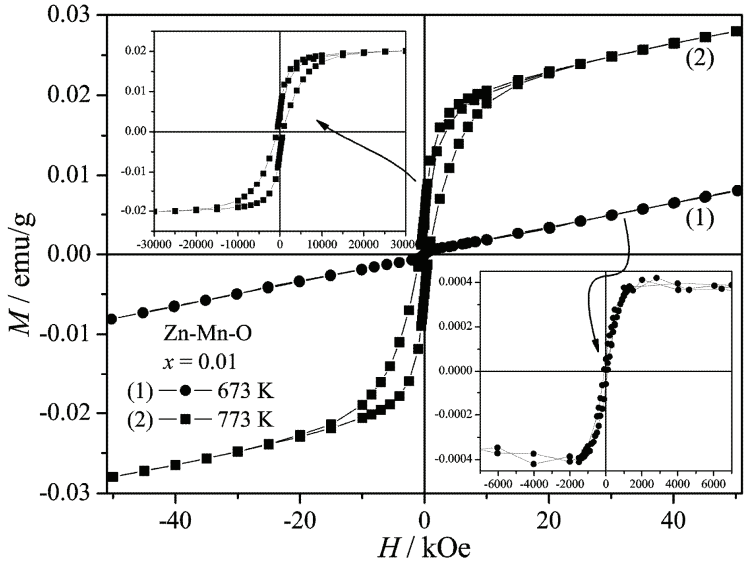

Fig. 8. Field dependent magnetization curves for the Zn–Mn–O samples with x = = 0.01 thermally treated at: 673 (1) and 773 K (2). The insets show the ferromagnetic component of the magnetization obtained after subtracting the paramagnetic contribution.

Contrary to these observations, there was no RT ferromagnetism in the x = = 0.10 sample thermally treated at 773 K nor in the x = 0.01 sample thermally treated at 1173 K. The $M(H)$ dependence for these samples was a linear function in the magnetic field range up to 50 kOe, indicating the paramagnetic origin of the magnetization at 300 K.

The EPR spectra of the studied Zn–Mn–O samples at 300 K are presented in Fig. 9. A broad resonance appeared in the x = 0.01 and 0.04 samples thermally treated at 773 K on the lower field side, which was absent in the x = 0.10 sample thermally treated at 773 K and in the x = 0.01 sample thermally treated at 1173 K. The broad resonance is attributed to ferromagnetic phase in the material. The EPR spectrum in the form of fine and hyperfine lines was detected on the higher field side in all the investigated Zn–Mn–O samples (Fig. 9). This spectrum was analysed by the following spin-Hamiltonian:

$$H = g\mu_B \mathbf{HS} + D\left[S_z^2 - \tfrac{1}{3}S(S+1)\right] + A\mathbf{SI} \qquad (1)$$

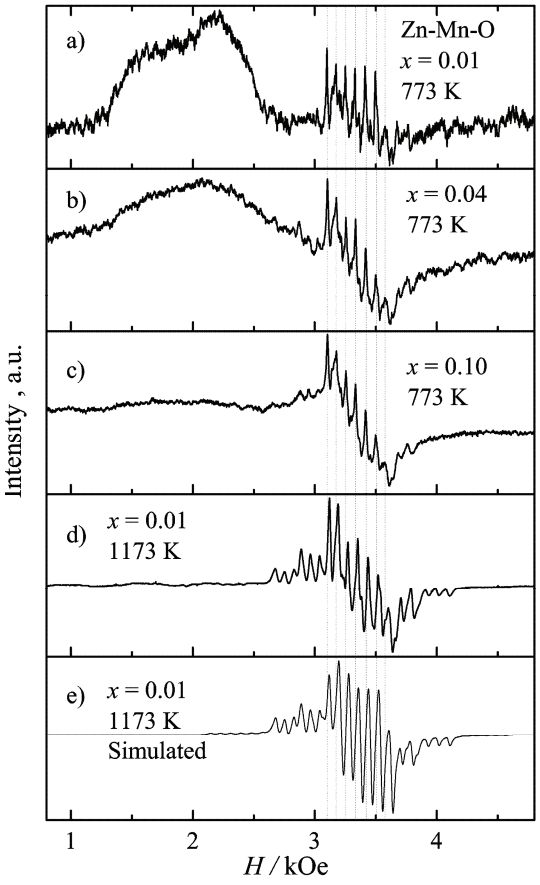

Fig. 9. EPR Spectra of the Zn–Mn–O samples: a) x = 0.01 thermally treated at 773 K, b) x = 0.04 thermally treated at 773 K, c) x = 0.10 thermally treated at 773 K, d) x = 0.01 thermally treated at 1173 K, e) simulated spectrum of Mn^{2+} with S = 5/2 and I = 5/2 in the ZnO crystal lattice (EPR parameters used in the simulation are A = –81 G, D = –252 G, g = 2.01).

where the first term describes the Zeeman interaction, the second term describes the axial zero-field splitting due to the hexagonal symmetry of the wurtzite ZnO and the third term describes the hyperfine interaction between the electron and nuclear spins of the manganese ions. For the Mn^{2+}, $S = 5/2$, there are five fine transitions in the magnetic field **H**. Each fine transition has six hyperfine transitions due to the hyperfine interaction of the Mn^{2+} electron spin and its nuclear spin, ^{55}Mn ($I = 5/2$). Good agreement with the experimental spectrum for the sample $x = 0.01$ thermally treated at 1173 K was obtained in the simulation using the spin-Hamiltonian parameters $A = -81$ G, $D = -252$ G and $g = 2.01$, Fig. 9e. These values agree well with the spin-Hamiltonian parameters ($A = -81$ G, $D = -232$ G and $g = 2.0016$) reported for a Mn^{2+} doped ZnO single crystal.[17,18] Thus, the EPR spectrum appearing in all the investigated Zn–Mn–O samples arises from the paramagnetic moments of isolated Mn^{2+} substitutionally incorporated into the ZnO crystal lattice. The isolated (uncoupled) Mn^{2+} do not contribute to the RT ferromagnetism.

Taking into account the manganese concentration in the $x = 0.01$ sample determined by an atomic absorption method, which was only a little less than that used in the synthesis, ≈ 0.8 at. %, and the measured saturation magnetization of the ferromagnetic phase in the sample thermally treated at 773 K, the average magnetic moment per Mn ion was found to be 0.03 μ_B/Mn at 300 K. A small value of the average magnetic moment per Mn ion was reported for bulk Mn-doped ZnO,[4,19] and in Mn-doped ZnO nanoparticles.[15]

TEM Analysis indicated that the coalescence of some zinc oxide and manganese oxide crystallites might cause microstructural changes (Fig. 6). It is very likely that at these locations, diffusion of zinc atoms into manganese oxide occurred. Clear evidence of this process is the appearance of the impurity phase in the thermally treated Zn–Mn–O samples detected by XRD analysis, which was identified as $Zn_{1-y}Mn_yMn_2O_4$ in the $x = 0.01$ sample and as a $ZnMn_2O_4$ phase in the $x = 0.10$ sample. The reverse process of diffusion of manganese atoms into the zinc oxide crystallites also occurred. Substitutional incorporation of Mn^{2+} into the ZnO crystal lattice was recorded in the EPR spectra. It was found that isolated Mn^{2+} in the ZnO crystal lattice do not contribute to the RT ferromagnetism. Nor does the RT ferromagnetism originate from the $ZnMn_2O_4$ phase. The $ZnMn_2O_4$ phase with tetragonal symmetry was observed in the $x = 0.10$ sample thermally treated at 773 K but RT ferromagnetism was not detected in this sample. The same applies to the $Zn_{1-y}Mn_yMn_2O_4$ phase. This impurity phase detected in the $x = 0.01$ sample progressively developed with increasing temperature of thermal treatment up to the highest temperature used in the sintering procedure, 1173 K, but the $x = 0.01$ sample thermally treated at 1173 K was fully paramagnetic at 300 K.

In addition to $Zn_{1-y}Mn_yMn_2O_4$, another secondary phase, MnO_2, was detected in the $x = 0.01$ sample thermally treated at 773 K. This manganese oxide is antiferromagnetic with a Néel temperature about 84 K.[20] Pure MnO_2 transforms into Mn_2O_3 at about 773 K (Fig. 4). Pure Mn_2O_3 is also antiferromagnetic with a Néel temperature between 80 and 100 K.[21] In the presence of Zn atoms in Mn_2O_3, incorporation of Zn into Mn^{3+} sites is possible (the ionic radius of Zn^{2+} is about 0.60 Å and the ionic radius of Mn^{3+} is about 0.58 Å)[22] and this process causes oxygen release for charge neutrality and formation of vacancies in the Mn_2O_3 structure. It is interesting to note that incorporation of Zn into Mn_3O_4, where Zn substitutes Mn^{2+} in the cation sublattice, leads to low-temperature ferrimagnetisms similar to that of Mn_3O_4 but with a lower Curie temperature.[7] In the present investigation, RT ferromagnetism commenced to develop in the $x = 0.01$ sample thermally treated at 673 K, Fig. 8. At this temperature (673 K), a large part of the zinc oxalate had decomposed into ZnO. The abrupt increase of the ferromagnetic component of the magnetization in the $x = 0.01$ sample thermally treated at 773 K compared with that appearing at 673 K could be connected with the development of the Mn_2O_3 phase observed in the XRD pattern, Fig. 1, where the creation of oxygen vacancies due to presence of Zn atoms was expected. An oxygen-vacancy-stabilized metastable phase in the form $Mn_{2-x}Zn_xO_{3-\delta}$ was suggested as a possible source of the high-temperature ferromagnetism in the low-temperature processed Zn–Mn–O samples.[7] In several detailed studies, the diffusion of Zn atoms into the manganese oxides was also considered to be responsible for the observed high-temperature ferromagnetism in the low-temperature processed Zn–Mn–O bulk and some thin film multilayer samples.[23,24]

However, in a recently published paper, RT ferromagnetism in $Zn_{1-x}Mn_xO$ thin films grown by pulsed laser deposition was observed even in those samples ($x < 0.03$) which had no secondary phases.[25] The appearance of the Mn_2O_3 phase aggregating at grain boundaries was found for a higher Mn concentration, $x = 0.05$, but this sample exhibited smaller saturation magnetization than that recorded for the thin films with lower manganese content. These results suggest that the high-temperature ferromagnetism in Zn–Mn–O is not necessarily related to manganese oxides or other impurity phases and that this phenomenon is an intrinsic property of Mn-doped ZnO materials. It was established in the present study that the solubility of Mn in low-temperature processed bulk ZnO was low and that manganese oxides existed even in the Zn–Mn–O sample with $x = 0.01$ Mn doping.

There is a possibility that a fraction of the Mn ion magnetic moments incorporated in the ZnO crystal lattice in the $x = 0.01$ sample thermally treated at 773 K was ordered ferromagnetically at RT and that the ferromagnetically coupled moments co-existed with the paramagnetic moments of the isolated Mn ions (Fig. 9a). The coexistence of ferromagnetically coupled Mn ion moments and

paramagnetic moments of isolated Mn ions was found in a $Zn_{1-x}Mn_xO$ thin film sample with $x = 0.01$,[25] and in 2 at. % Mn-doped ZnO nanocrystals with an average particle size 12 nm annealed at 673 K.[15] This possibility focuses attention on free charge carriers as mediators in the ferromagnetic ordering. Theoretical models identified *p*-type ZnO doped with Mn as a ferromagnetic semiconductor with a high T_C.[1–3] It is now well known that nitrogen is one of the most effective *p*-type doping agents in ZnO.[26] A film prepared from nitrogen-capped nanocrystals of 0.2 at. % Mn^{2+}:ZnO exhibited saturation magnetization of the ferromagnetically coupled Mn^{2+} moments of 0.75 μ_B/Mn at 300 K.[5] In a Mn-doped ZnO bulk sample with $x = 0.3$ at. % Mn prepared from ZnO and MnO_2 precursors by a sintering procedure at 773 K in air, a ferromagnetic ordering of the uniformly distributed Mn^{2+} moments was observed with a saturation magnetization of 0.16 μ_B/Mn.[4] It should be noted that a bulk Zn–Mn–O sample with 1.0 % Mn sintered at 773 K under vacuum exhibited weaker ferromagnetic properties at RT than the sample with 1.0 % Mn sintered at 773 K in air.[8] Contrary to this observation, the thermal treatment of a bulk $Zn_{1-x}Mn_xO$ sample with $x = 0.02$ at 873 K in an argon atmosphere resulted in considerably stronger ferromagnetic properties at 300 K than those for the sample sintered at the same temperature in air.[19] In a recent study of the electrical properties of nitrogen-doped ZnO thin films, it was found that the introduction of Ar in the growth ambient enhanced the hole concentration and improved the conductivity of N-doped ZnO.[26] In the present study, the Zn–Mn–O sample with $x = 0.01$ prepared by the solid state sintering route, which was not intentionally doped with any kind of impurity, and with a final thermal treatment at 773 K in air, the saturation magnetization of the ferromagnetic phase was estimated to be 0.03 μ_B/Mn at 300 K. The very small value of the average magnetic moment per Mn ion in this ferromagnetic sample was partly the consequence of the small fraction of Mn ions participating in the ferromagnetic ordering. The common property of almost all the Zn–Mn–O samples prepared either in the bulk form by a solid state reaction method[4,7,8,22,24] or in the form of thin films,[4] or in the form of nanocrystalline particles[15] is that the RT ferromagnetism appeared in the low-temperature processed samples (673–873 K) and was absent in samples exposed to high-temperature treatment (above 1073 K). The magnetic properties of the Zn–Mn–O samples observed in the present study, as well as those reported by other authors, indicate that these properties are extremely sensitive to the conditions of sample preparation, where the type and concentration of defects play a very important role.

According to a theoretical study of the hole mediated ferromagnetism in Mn^{2+}:ZnO, the 3d electrons of Mn^{2+} were predicted to delocalize partially into the shallow acceptor states, thus providing exchange interaction and ferromagnetic coupling between the Mn ions.[1] Taking into consideration the conditions of synthesis of the low-temperature processed Zn–Mn–O samples in this study, it

seems that the observed RT ferromagnetism could originate from interactions between the Mn^{2+} and uncompensated acceptor defects incorporated in the ZnO crystal lattice during the thermal treatment of the samples.

CONCLUSIONS

Room temperature ferromagnetism was observed in Zn–Mn–O samples with $x = 0.01$ thermally treated at 673 and 773 K, and in the $x = 0.04$ sample thermally treated at 773 K. The structural and magnetic properties of the Zn–Mn–O samples showed that they were non-homogeneous materials. An analysis of the experimental results of this work suggests that the observed RT ferromagnetism in the low-temperature processed samples could arise from interactions between the Mn^{2+} and *p*-type defects incorporated in the ZnO crystal lattice during the thermal treatment of the samples.

Acknowledgments. Financial support for this study was granted by the Ministry of Science and Technological Development of the Republic of Serbia, Projects No. 141013 and 141027.

И З В О Д

ФЕРОМАГНЕТНО ПОНАШАЊЕ Zn–Mn–O СИСТЕМА

БРАНКА БАБИЋ-СТОЈИЋ, ДУШАН МИЛИВОЈЕВИЋ и ЈОВАН БЛАНУША

Институт за нуклеране науке "Винча", п. пр. 522, 11001 Београд

Поликристални узорци Zn–Mn–O номиналних концентрација мангана x = 0,01, 0,04 и 0,10 добијени су реакцијом у чвстом стању између $(ZnC_2O_4{\cdot}2H_2O)_{1-x}$ и $(MnC_2O_4{\cdot}2H_2O)_x$. Термички третман је извршен на ваздуху и температурама 673, 773, 873, 973 и 1173 K за x = 0,01 и на температури 773 K за x = 0,04 и 0,10. Узорци су испитивани методама дифракције x-зрака на праху, термогравиметрије, диференцијалне термалне анализе, трансмисионе електронске микроскопије, мерења магнетизације и електронске парамагнетне резонанце. Методом дифракције x-зрака на праху су испитани и узорци MnO_2 термички третирани на температурама 673, 773, 873, 973, 1073 и 1173 K. Феромагнетизам на собној температури је уочен у Zn–Mn–O узорцима концентрације мангана x = 0,01 термички третираним на ниским температурама (673 и 773 K) и у узорку x = 0,04 термички третираном на 773 K. Резултати указују на то да би феромагнетизам могао да буде последица интеракције између Mn^{2+} и акцепторских дефеката уграђених у кристалну решетку ZnO за време термичког третмана узорака.

(Примљено 26. маја, ревидирано 16. јула 2008)

REFERENCES

1. T. Dietl, H. Ohno, F. Matsukura, J. Cibert, D. Ferrand, *Science* **287** (2000) 1019
2. K. Sato, H. Katayama-Yoshida, *Japan J. Appl. Phys*. **39** (2000) L555
3. K. Sato, H. Katayama-Yoshida, *Semicond. Sci. Technol*. **17** (2002) 367
4. P. Sharma, A. Gupta, K. V. Rao, F. J. Owens, R. Sharma, R. Ahuja, J. M. Osorio Guillen, B. Johansson, G. A. Gehring, *Nat. Mater*. **2** (2003) 673
5. K. R. Kittilstved, N. S. Norberg, D. R. Gamelin, *Phys. Rev. Lett*. **94** (2005) 147209
6. A. Manivannan, P. Dutta, G. Glaspell, M. S. Seehra, *J. Appl. Phys*. **99** (2006) 08M110

7. D. C. Kundaliya, S. B. Ogale, S. E. Lofland, S. Dhar, C. J. Metting, S. R. Shinde, Z. Ma, B. Varughese, K. V. Ramanujachary, L. Salamanca-Riba, T. Vankatesan, *Nat. Mater*. **3** (2004) 709
8. J. Zhang, R. Skomski, D. J. Sellmyer, *J. Appl. Phys*. **97** (2005) 10D303
9. S. Kolesnik, B. Dabrowski, J. Mais, *J. Appl. Phys*. **95** (2004) 2582
10. G. Lawes, A. S. Risbud, A. P. Ramirez, R. Seshadri, *Phys. Rev*. **B71** (2005) 045201
11. H. W. Zhang, E. W. Shi, Z. Z. Chen, X. C. Liu, B. Xiao, *Solid State Commun*. **137** (2006) 272
12. A. Tiwari, C. Jin, A. Kvit, D. Kumar, J. F. Muth, J. Narayan, *Solid State Commun*. **121** (2002) 371
13. T. Fukumura, Z. Jin, M. Kawasaki, T. Shono, T. Hasegawa, S. Koshihara, H. Koinuma, *Appl. Phys. Lett*. **78** (2001) 958
14. S. W. Jung, S. J. An, G. C. Yi, C. U. Jung, S. I. Lee, S. Cho, *Appl. Phys. Lett*. **80** (2002) 4561
15. O. D. Jayakumar, H. G. Salunke, R. M. Kadam, M. Mohapatra, G. Yaswant, S. K. Kulshreshtha, *Nanotechnology* **17** (2006) 1278
16. S. J. Pearton, W. H. Heo, M. Ivill, D. P. Norton, T. Steiner, *Semicond. Sci. Technol*. **19** (2004) R59
17. P. B. Dorain, *Phys. Rev*. **112** (1958) 1058
18. A. Hausmann, H. Huppertz, *J. Phys. Chem. Solids* **29** (1968) 1369
19. W. Chen, L. F. Zhao, Y. Q. Wang, J. H. Miao, S. Liu, Z. C. Xia, S. L. Yuan, *Appl. Phys. Lett*. **87** (2005) 042507
20. B. D. Cullity, *Introduction to Magnetic Materials*, Addison–Wesley Publishing Company, Merlo park, CA, 1972, p. 157
21. M. Regulski, R. Przeniosło, I. Sosnowska, D. Hohlwein, R. Schneider, *J. Alloys Compounds* **362** (2004) 236
22. K. P. Bhatti, S. Chaudhary, D. K. Pandya, S. C. Kashyap, *Solid State Commun*. **136** (2005) 384
23. J. L. Costa-Krämer, F. Briones, J. F. Fernández, A. C. Caballero, M. Villegas, M. Díaz, M. A. García, A. Hernando, *Nanotechnology* **16** (2005) 214
24. M. A. García, M. L. Ruiz-Gonzáles, A. Quesada, J. L. Costa-Krämer, J. F. Fernández, S. J. Khatib, A. Wennberg, A. C. Cabarello, M. S. Martín- Gonzáles, M. Villegas, F. Briones, J. M. Gonzáles-Calbet, A. Hernando, *Phys. Rev. Lett*. **94** (2005) 217206
25. J. Zhang, X. Z. Li, J. Shi, Y. F. Lu, D. J. Sellmyer, *J. Phys. Condens. Matt.* **19** (2007) 036210
26. J. Lu, Q. Liang, Y. Zhang, Z. Ye, S. Fujita, *J. Phys. D: Appl. Phys.* **40** (2007) 3177.